Arch. Min. Sci. **66** (2021), 4, 495-509

Electronic version (in color) of this paper is available: http://mining.archives.pl

DOI: https://doi.org/10.24425/ams.2021.139593

JAKUB JANUS[1*]

AIR FLOW MODELLING ON THE GEOMETRY REFLECTING THE ACTUAL SHAPE OF THE LONGWALL AREA AND GOAFS

The article presents a numerical model of a U-ventilated longwall, taking into account detailed elements such as arch yielding support, roof supports and shearer. What distinguishes it from previous models is the mapping of adjacent goafs. This model considers the current state of knowledge regarding spatial height distribution, porosity and permeability of goafs. Airflow calculations were carried out using the selected turbulence models to select appropriate numerical methods for the model. Obtained results show possibilities of conducting extensive numerical calculations for the flow problems in the mine environment, taking into account more complex descriptions and the interpretation of the calculation results carried out with simpler models.

Keywords: mine ventilation, goafs, CFD, numerical model, air flow velocity

1. Introduction

A few years ago, it was not possible to carry out numerical calculations on geometries reflecting the actual shape of the longwall area, including the longwall equipment and goafs. One of the main stages in constructing such a geometric model is meshing, which must meet the appropriate quality requirements. The computational mesh should be condensed near the model's walls to ensure the appropriate dimensionless length parameter $y+$, which is a verification of the node located at a distance from the numerical geometry walls. It is recommended that within the boundary layer should be at least 5 cells with a size ensuring $y+$ in the range $30 \sim 50 \leq y+ \leq 500$. It is stated [7] that the optimal value of the $y+$ parameter should be in the range $y+ = 40 \sim 100$. Another criterion determining the quality of the computational mesh is the skewness coefficient, *Sk*.

[1] STRATA MECHANICS RESEARCH INSTITUTE, 27 REYMONTA STR., 30-059 KRAKÓW, POLAND

* Corresponding author: janus@imgpan.pl

The default method of determining the skewness coefficient for tetrahedral cells is the equilateral volume method. This parameter is defined as the difference between the shape of the cell and the shape of an equilateral cell of equivalent volume. The skewness coefficient determines how close the cell is to the ideal in terms of equal sides and equal angles.

Assuming the above quality criteria for applying a correct numerical mesh ta geometric model that reflects the real object, it is inevitable to obtain a computational grid with a size of several or several dozen million cells. Such elements require a unit with high computing power, but also significantly extends the time of the calculations themselves. Therefore, the resulting limitations somehow force users to make significant simplifications in model geometry.

The same situation can be observed in CFD tasks performed for the needs of Mining Aerology. The complexity of the longwall area geometry and goafs has not made it possible yet, to accurately reflect their shapes to carry out numerical calculations. In the vast majority of previous CFD calculations, both the longwall and the goafs were presented as rectangular areas with constant dimensions, not considering the presence of arch yielding support, roof supports and shearer, etc. Classic measurement methods require a significant investment of time and effort of many people, who frequently work in conditions that pose a threat to their health and lives. One of such measurement techniques is Terrestrial Laser Scanning, which, due to the increasing availability of equipment and its prices, becomes one of the basic measurement technologies. Using the laser scanning technology in underground mining made it possible to quickly obtain information about the measured object geometry for inventory and geodetic purposes, while maintaining the required accuracy [2,7-9,23]. This information is already successfully used for the construction of numerical models for mining aerology problems [6].

In the case of goafs mapping, it is not possible to use the available measurement techniques to accurately map the shape, therefore this area is also simplified in numerical calculations. One of the works presenting the simplified numerical geometry model is the article P. Skotniczny [22], where the longwall and mine drift had a constant geometry with a rectangular cross-section shape. Although this model took into account the presence of goafs, their shape was significantly simplified. Due to these simplifications, the model was discretised with a quad-type structural mesh. A similar situation occurs in the article by K. Wierzbicki [26], in which the author presents the influence of the mine drift geometry on the methane concentration distribution in the longwall area. Presented numerical geometry, which is a part of a longwall with goafs is also significantly simplified. The geometry of the goafs corresponds to the shape of a cube with a rectangular cross-section, as does the longwall shape, which additionally does not take into account the presence of mining equipment.

The described geometric model of goafs did not take into account the variable goafs height, shape and changes in the porosity and permeability parameters. By introducing appropriate dependencies into the three-dimensional model of the area, it is possible to fully use the available experimental data and assess to what extent the simplifying assumptions affect the results of the flow simulations in goafs.

Calculations were carried out using the finite volume method implemented in the ANSYS Fluent software. A three-dimensional model was considered for an area including a longwall, maingate, tailgate and goafs. Calculations were carried out for the issue of non-stationary turbulent flow using k-e turbulence models. Descriptions were formulated in accordance with generally accepted principles of good practice [18,19], data from the literature and own experiences, largely verified by in-situ measurements [16].

2. Numerical research

To carry out numerical calculations of the airflow through the longwall and goafs, a geometric model of longwall ventilated with the "U" system from the boundaries of the mining field was designed. In this ventilation system, fresh air is supplied to the longwall by the maingate and discharged through the tailgate. Mine drifts are maintained only along the coal face, hence the air stream is in contact with the goafs only along the length of the longwall. Therefore, with this system, there is limited airflow through the goafs [25].

2.1. Numerical model geometry

The geometric model included maingate 3.8 m high, 5.5 m wide (cross-sectional area 17 m^2) and 29.0 long (Fig. 1). At a distance of 10.0 m from the inlet, the maingate connects to the longwall inlet, 6.6 m wide, 2.9 m high, 90.0 m long with a slope of 8° (Fig. 2). The longwall shearer was located at a length of 55.0 m, and the cutting direction corresponds to the direction of airflow in the longwall. The longwall connects to the tailgate, 3.8 m high, 5.5 m wide (cross-sectional area 17 m^2) and 47.0 m long. The model also takes into account the presence of goafs with a length of 60.0 m.

The goafs height area was determined using the approximation functions presented in the monograph [5]. Goaf's height changes in the surface perpendicular to the coal face presented by the function

$$h(x) = c\left(1 - 2e^{-ax} + e^{-bx}\right) + g_r \tag{1}$$

where:

c, a, b — approximation coefficients,
g_r — longwall height,
x — goafs coordinate in the x-axis direction.

It should be noted that the above function may not apply to all coal-bearing strata in the world, but mainly, European geology.

Constants a, b and c are determined by the following formulas:

$$c = 1.45\, g_r \tag{2}$$

$$e^{-bx_{h\max}} - 2e^{-ax_{h\max}} = \frac{2.5}{1.45} - 1 \tag{3}$$

$$X_{h\max} = \frac{1}{(b-4)} \ln \frac{b}{2a} \tag{4}$$

where: $x_{h\max}$ — maximum goafs height coordinate.

The solution of set equations (3) and (4) made it possible to calculate the values of a and b constants .

Goafs height changes in the parallel surface to the coal face are presented as:

$$h_{1+2}(y) = a_y\left[1-\left(\frac{2}{L}y-1\right)^4\right]+\left(1-a_y\right)\left[1-\left(\frac{2}{L}y-1\right)^4\right] \tag{5}$$

where:

L — longwall length,
y — goafs coordinate in the y-axis direction.

The a_y coefficient appearing in the equation (5) determines the shape variable of the function (5). The changes of the a_y coefficient as a function of distance x are approximated by the following equation:

$$a_y = \left(a_{y0}-1\right)e^{-\tau x}+1 \tag{6}$$

where:

τ — time constant of a_y function,
a_{y0} — initial value that fulfill conditions $0 \le a_{y0} \le 1$.

The a_{y0} coefficient depends on the properties of the roof rocks, according to the classification given by A. Kidybińskiego [14] and modified in the work of J. Szlązaka [24].

It was assumed that the maximum goafs height is at a distance of $x_{h\,\max} = 50.0$ m. For this value of $x_{h\,\max}$, the values of the constants $a = 0.0722$, $b = 0.00501$ were calculated from the formulas (3) and (4). For this example of goafs, the 1st class of the roof rocks, formed by clay shales, it was assumed that the initial value $a_{y0} = 0.2$. Using the formulas (1) and (5), the goafs height variability course was determined. The shape of goafs is presented in the figures (Fig. 1), (Fig. 2).

In order to map the actual conditions in mine drifts, it was decided to simplify the geometry model as little as possible. Therefore, the geometric model accounted for such elements as arch

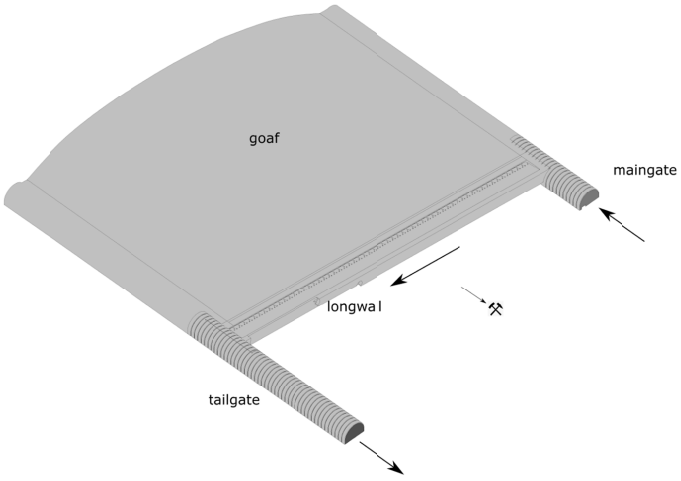

Fig. 1. Geometric model of the longwall, ventilated with the "U" system from the boundaries of the mining field

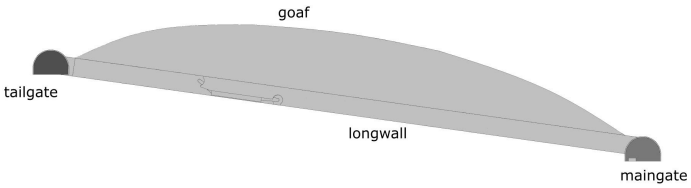

Fig. 2. Geometric model of the longwall, ventilated with the "U" system from the boundaries of the mining field, view from the coal face

yielding support and scraper conveyor in the maingate, roof supports, shearer and scraper conveyor in longwall, arch yielding support and ventilation partition in the tailgate (Fig. 3), (Fig. 4).

The entire model of the roof supports in longwall has been simplified, which resulted from the necessity to limit the number of details that significantly affect the time of generating the mesh elements.

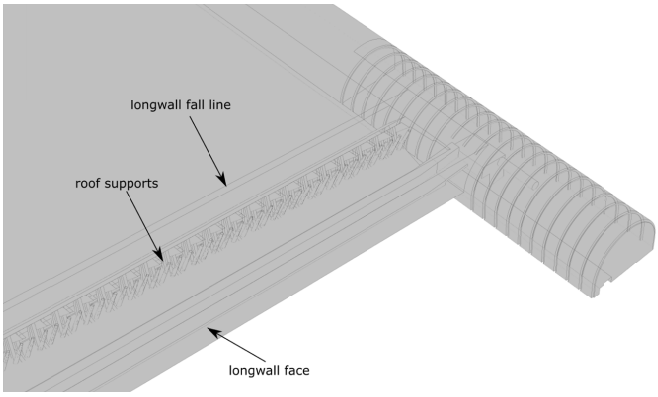

Fig. 3. Diagram of the intersection of the maingate with the longwall

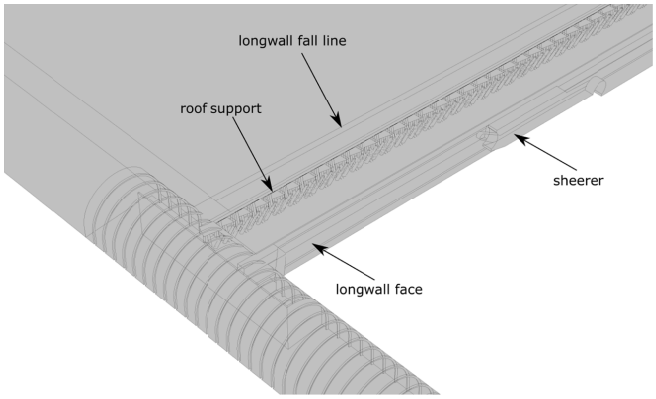

Rys. 4. Diagram of the intersection of the longwall with the tailgate

2.2. Numerical mesh

Due to the presence of two areas with different types of flow in the numerical model
- goaf area (laminar flow),
- maingate, longwall, tailgate (turbulent flow),

it was necessary to apply numerical mesh with different cell sizes.

However, using equal mesh over the entire calculation model would significantly extend time calculations. It was decided to use the size function, which allows you to control mesh size around the selected point, edge or surface.

In the area of turbulent flow, where the flow direction is difficult to predict, it is justified to impose dense numerical mesh. During the mesh independence study, consisting in discretising numerical mesh of different densities on the tested section of the model [12], the mesh parameters were selected, given results of numerical calculations similar to the results of the calculations for the mode dense mesh. Therefore, a mesh with the following parameters is applied to the area of the maingate, longwall and tailgate:
- minimum mesh size 7.0 cm,
- maximum mesh size 20.0 cm,
- growth rate 1.2.

The goafs area, which is a porous medium in which laminar flow occurs, was digitis ed with a mesh with the following parameters:
- minimum mesh size 50.0 cm,
- maximum mesh size 200.0 cm,
- growth rate 1.2.

The geometry of the numerical model was discretis ed with a non-structural tetrahedral mesh, which was then converted into a polyhedral mesh (Fig. 5).

The designed numerical mesh consisted of 20.9 million tetrahedral cells. After conversion to a polyhedral mesh, the number of cells decreased to 5.1 million.

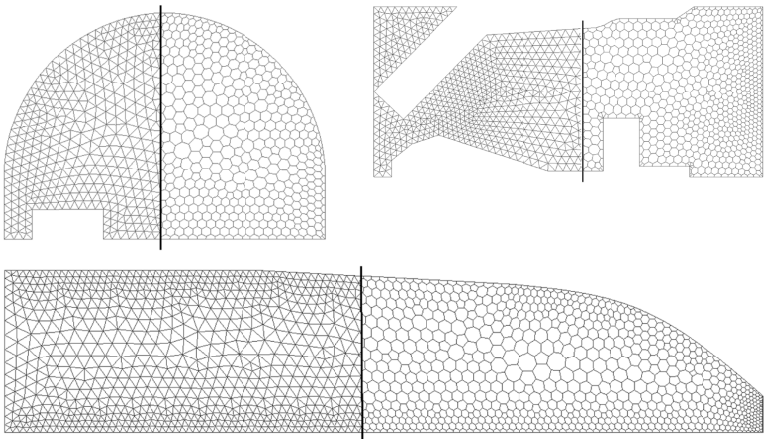

Fig. 5. View of the mesh before and after the conversion in the area of maingate, longwall face, and goafs

To determine the quality of the generated numerical mesh, the skewness coefficient *Sk* was used.

According to the definition of the skewness coefficient, the value 0 means an equilateral cell, and the value 1 is a very bad cell characterised by nodes located almost on one surface [1].

The skewness factor for the numerical grid with presented parameters is shown in table 1 in the form of a percentage share of grid cells in a specific range of skewness factor.

TABLE 1

Percentage share of numerical grid cells for skewness factor ranges

Skewness factor	Percentage share [%]	Cell quality
1	0.0	poorest
0.9 < 1	0.0	very poor
0.75 – 0.9	0.0	poor
0.5 – 0.75	10.1	moderate
0.25 – 0.5	52.5	good
0 > 0.25	33.9	top
0	3.5	equilateral

A dimensionless parameter of length $y+$ for the computational area falls within a range of $10 \leq y+ \leq 440$. The number of cells within a range of $10 \leq y+ \leq 30$ is small, which allows for the acceptance of the grid quality in terms of a dimensionless parameter of length $y+$.

2.3. Boundary conditions

The initial calculations enabled the generation of the boundary conditions at the inlet to the model. These calculations were carried out for a 30 m straight section of a mine drift with the same geometry corresponding to the inlet section of the main model. The developed velocity profile was generated by the iterative method, starting with the assumption of the flat profile with average velocity $V = 1.0$ m/s at the inlet, which gave 1020 m^3/min of fresh air inflow. In this condition, the total pressure is not constant but is adjusted to the value necessary to ensure the specified velocity distribution. The profile at the end of the model was the first approximation of the unfolded profile. In the following calculations, this profile was applied at the inlet. The iteration process was repeated several times until a satisfactory convergence was obtained [4,11,28,], Obtained developed profile was set as a boundary condition for the main model.

The outlet has been defined as outflow, corresponding to the outflow model in which it does not define the velocity or pressure conditions [10,20]. The floor, arches, longwall face and sheerer were defined as wall surfaces. Inequalities of the floor in the model were treated as roughness with a height of 0.05 m, and in the case of arches, rails and pipelines, a roughness height of 0.001 m [21,27].

The goafs parameters were determined using the approximation functions presented in the monograph [5]. The goaf's part of the numerical model was defined as a porous media with a constant porosity of $32 \cdot 10^{-8}$ m^2 and a constant permeability of 0.5. In the main part of the goafs, the flow was assumed to be laminar, while the possible effect of turbulent flow at the surface between longwall and goafs, were taken into account by adding the volume behind the roof support.

Additionally, to monitor changes in the airflow velocity in the longwall and tailgate, there are defined measuring points recording the air velocity with a frequency of 10 Hz (Fig. 6). There are three points in the longwall, located 30 m from the inlet, in the middle of the width of the passage between the roof support and scraper conveyor. In the vertical axis called longwall_p, the points are placed at an equal distance of 0.60 m from each other. In the tailgate, the points are located at a distance of 23.0 m behind the longwall outflow, on the horizontal axis called tailgate_p, at an equal distance of 1.37 m, on the height of 0.9 m. In the goafs, there were nine defined measurement points. The points on the vertical axis called goafs_p1 and goafs_p3, are located at a distance of 10.0 m from the longwall fall line and 10.0 m from the liquidated maingate and tailgate. Points are placed at an equal distance of 1.50 m from each other. Points on the vertical axis called goafs_p2, are located at a distance of 40.0 m from the longwall fall line and half the length of the longwall. The points are placed at equal distances of 3.20 m from each other.

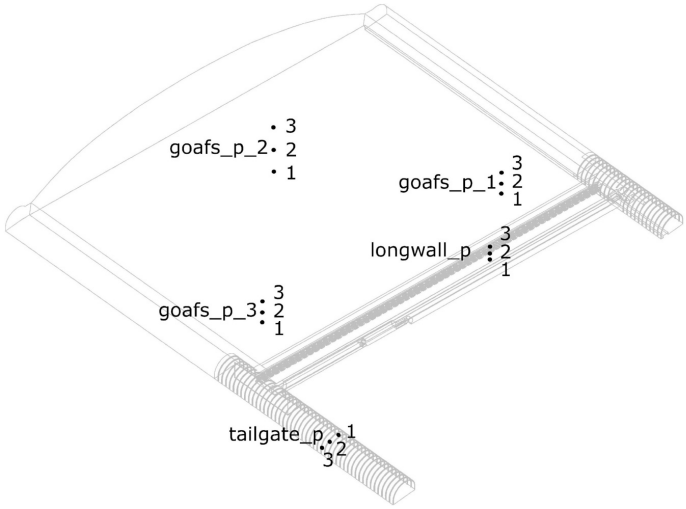

Fig. 6. Location of measurement points in the longwall, tailgate ang goafs

Due to the nature of the airflow in mine drifts and the large size of the computational grid, the turbulent flow was modelled using the *k*-*ε* model. It is a semi-empirical model based on the equations of kinetic energy transport of turbulence k and its dissipation *ε* [3]:

$$\frac{\partial}{\partial t}(\rho k)+\frac{\partial}{\partial x_i}(\rho k u_i)=\frac{\partial}{\partial x_j}\left[\left(\mu+\frac{\mu_t}{\sigma_k}\right)\frac{\partial k}{\partial x_j}\right]+R_{ij}\frac{\partial u_i}{\partial x_j}-\rho\varepsilon \tag{7}$$

$$\frac{\partial}{\partial t}(\rho\varepsilon)+\frac{\partial}{\partial x_i}(\rho\varepsilon u_i)=\frac{\partial}{\partial x_j}\left[\left(\mu+\frac{\mu_t}{\sigma_\varepsilon}\right)\frac{\partial \varepsilon}{\partial x_j}\right]+C_{1\varepsilon}\frac{\varepsilon}{k}R_{ij}\frac{\partial u_i}{\partial x_j}-C_{2\varepsilon}\rho\frac{\varepsilon^2}{k} \tag{8}$$

where: $C_{1\varepsilon}$, $C_{2\varepsilon}$, σ_k, σ_ε — constants.

Turbulent viscosity is determined from the equation:

$$\mu_T = \rho C_\mu \frac{k^2}{\varepsilon} \tag{9}$$

Constant parameters have been determined empirically:

$$C_\mu = 0.09 \quad C_{1\varepsilon} = 1.44 \quad C_{2\varepsilon} = 1.92 \quad \sigma_k = 1.0 \quad \sigma_\varepsilon = 1.3$$

In this model, the Reynolds stress tensor is represented as:

$$R_{ij} = \rho \overline{\hat{u}_i \hat{u}_k} = -\mu_T \left[\frac{\partial u_i}{\partial x_k} + \frac{\partial u_k}{\partial x_i} \right] + \frac{2}{3} \left(k + \mu_T \frac{\partial u_j}{\partial x_j} \right) \delta_{ik} \tag{10}$$

Or in a mode simplified form for isochoric flows:

$$R_{ij} = \rho \overline{\hat{u}_i \hat{u}_k} = -\mu_T \left[\frac{\partial u_i}{\partial x_k} + \frac{\partial u_k}{\partial x_i} \right] + \frac{2}{3} k \delta_{ik} \tag{11}$$

where: δ_{ik} — the Kronecker delta.

Calculations were carried out in an unsteady flow with a time step of 0.1 s. Solutions converge after less than 10 iterations per time step [13]. Residuals were $1 \cdot 10^{-5}$ for continuity and much smaller for other variables. Recommended for the *k-ε* model solutions methods, including second-order pressure and bounded central differencing for transient formulation have been applied. Calculations were performed until stabilisation of the time-averaged values.

2.4. Numerical simulation results of air flow in the area of the longwall and goafs

Numerical calculations were carried out until the fluctuations of average velocities at measurement points located in the longwall, tailgate, and goafs stabilised. By analysing the graphs of the recorded velocities for all measuring points, it is possible to observe the stabilisation of the flow around 100 seconds from the moment of starting the calculations.

During the analysis of the graphs, it is necessary to notice the difference in velocities between two extreme points, londwall_p1 and longwall_p2. At the point closer to the floor (longwall_p1), the airflow velocity is 1 m/s, while at the point closer to the roof (longwall_p3), this speed is 50% higher and amounts to about 1.5 m/s (Fig. 7).

Velocities recorded by the measurement points located in the tailgate show the influence of the longwall-tailgate intersection on the velocity profile (Fig. 8). The measurement points tailgate_p2 and tailgate_p3, located closer to the right side of a tailgate (looking in the flow direction), show a much higher airflow velocity than at the point tailgate_p1, located closer to the left side of a tailgate.

The measurement points located in the goaf area show the airflow velocity several times smaller than those recorded in the longwall and tailgate. The highest velocity was approximately 1.9 mm/s and was measured at points located near the longwall outlet (Fig. 11). In the case of

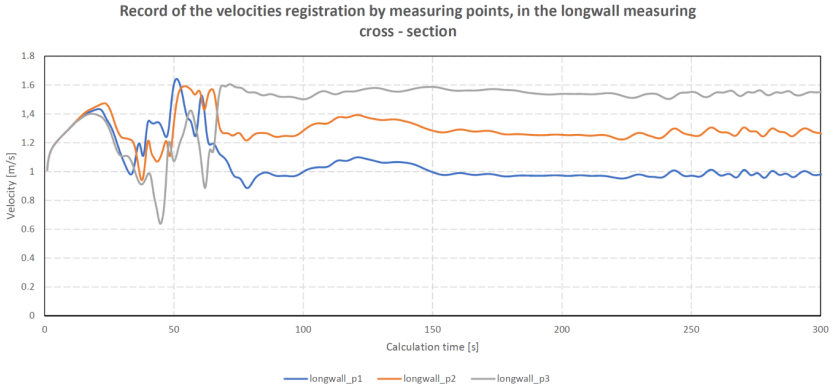

Fig. 7. Record of the velocities registration by measuring points, in the longwall measuring cross-section

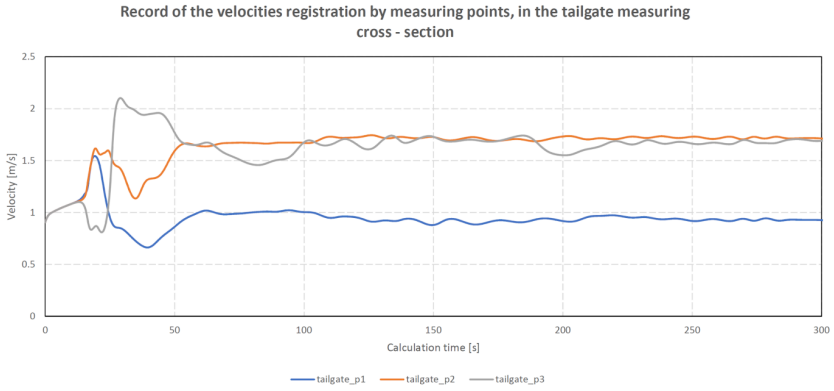

Fig. 8. Record of the velocities registration by measuring points, in the tailgate measuring cross-section

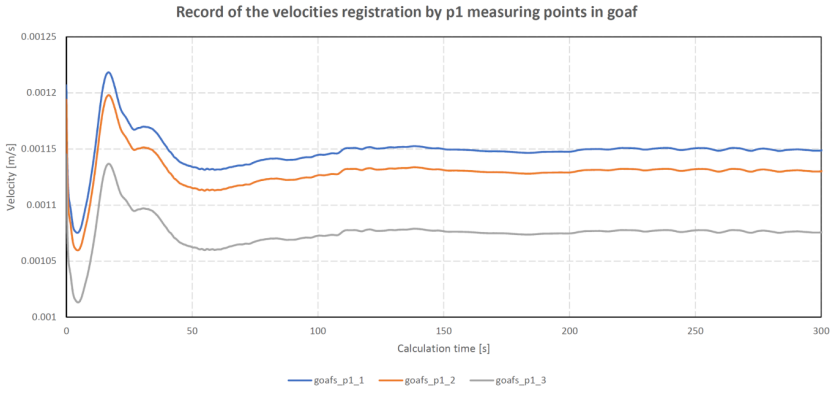

Fig. 9. Record of the velocities registration by p1 measuring points in goafs

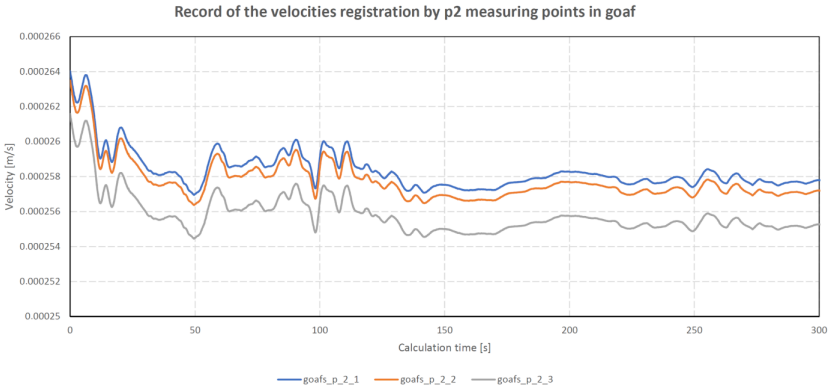

Fig. 10. Record of the velocities registration by p2 measuring points in goafs

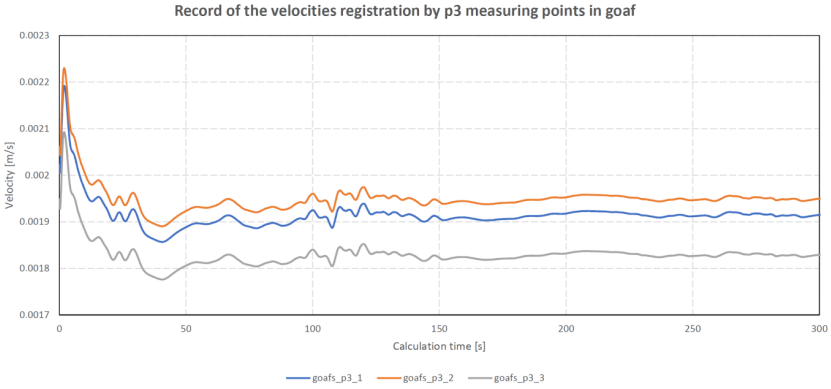

Fig. 11. Record of the velocities registration by p3 measuring points in goafs

the points located near the longwall inlet, the measured airflow velocity is 111.0 mm/s (Fig. 9). The lowest velocities, around 0.255 mm/s, were measured for the points located farthest from the longwall fall line (Fig. 10).

Figure 12 shows the velocity distribution contours for three-time moments of the calculations, 50 s, 100 s and 150 s. In the vicinity of the longwall inlet, the air stream is directed towards the longwall, more precisely to the roof supports area, reaching the airflow velocity to about 1.5 m/s. In the vicinity of the longwall shearer, by narrowing the cross-section, the airflow velocity increases to about 1.8 m/s. In the vicinity of the longwall outlet, the airflow velocity is above 2.0 m/s and reaches several meters from the tailgate.

During the analysis of the air velocity distributions in goafs, the highest velocities should be observed in the vicinity of the longwall outlet. Slightly lower ones can be seen in the vicinity of the longwall inlet (Fig. 13). These velocities reach a maximum of 10.0 mm/s. The lowest airflow velocities in goafs are located in the sections furthest away from the longwall fall line and amount to about 0.2 mm/s. Figure 14 shows the trajectory of the airflow (without the flow designation) through the longwall area and goafs.

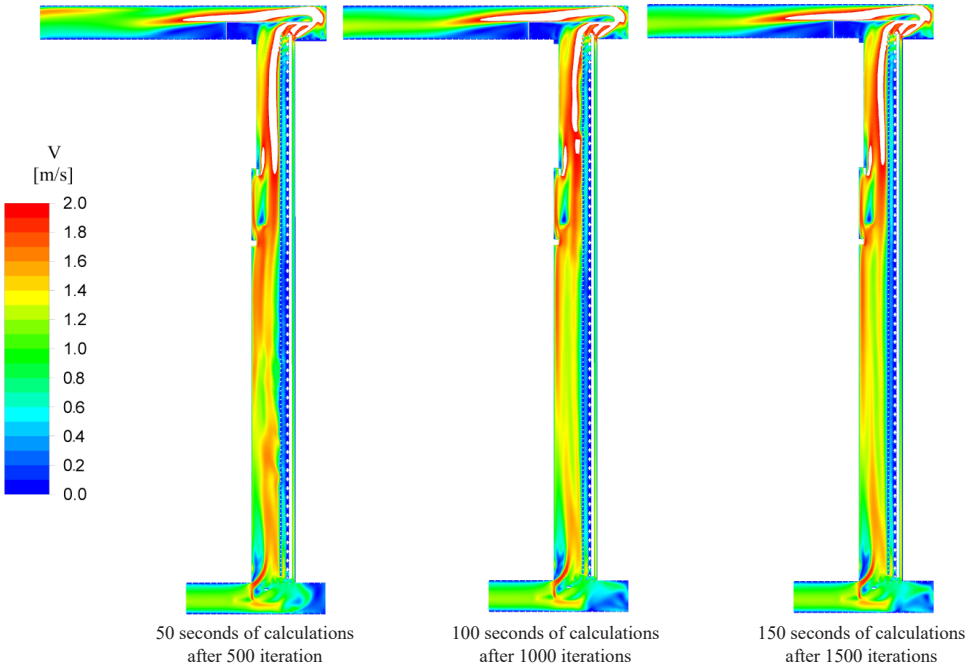

Fig. 12. Air velocity distribution in the range from 0.0 m/s to 2.0 m/s in the area of the longwall

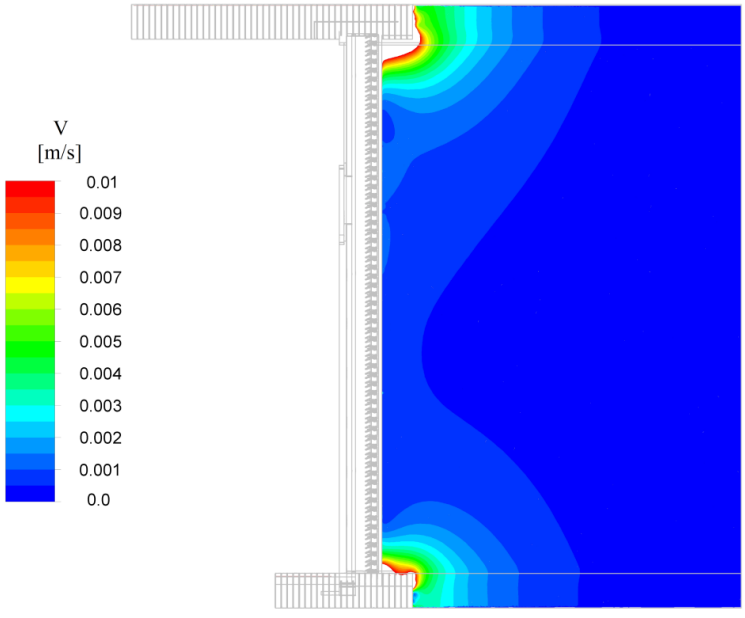

Fig. 13. Air velocity distribution in the range from 0,0 m/s to 0,01 m/s
in goaf after 150 seconds of calculations

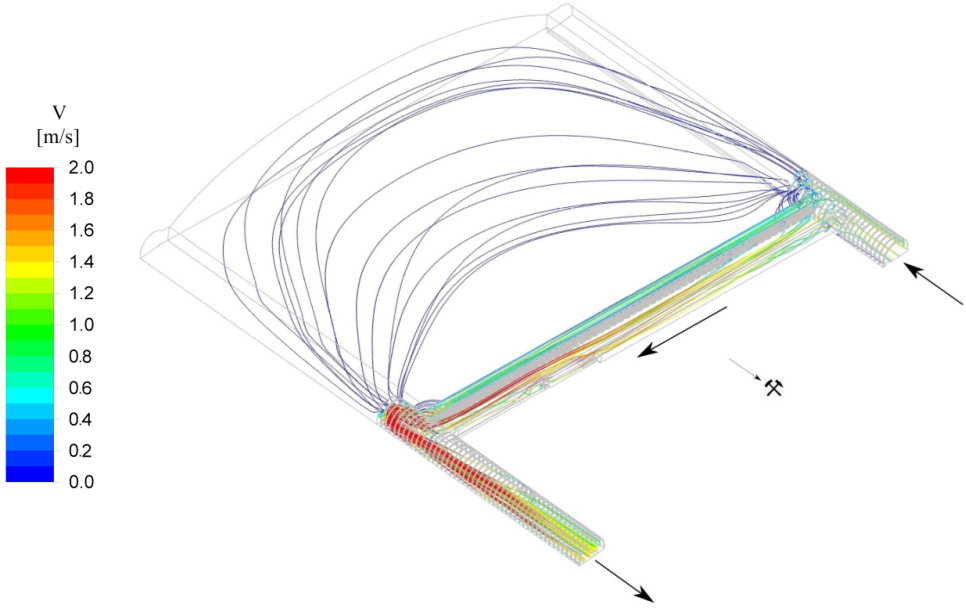

Fig. 14. Air flow trajectory in the range from 0.0 m/s to 2.0 m/s through the longwall area and goaf after 150 seconds of calculations

3. Conclusion

The article presents the calculation of airflow through the longwall area and goafs results. The designed model reflects the actual shape of a mine drift, including machines and equipment devices, as well as accurately reflects the shape of goafs.

The obtained results of numerical calculations allow us to observe the formation of the velocity profile in two areas with different types of flow:

- goaf's area,
- maingate, longwall and tailgate area.

Analysing the flow of clean air in mine drifts and goafs, reveals there are significant differences in the air velocity. The average flow velocity in the area of the mine drifts is about 1.0 m/s, while the flow velocity through the goaf's porous medium is less than 0.01 m/s.

In the following stages of work related to the task, the constant parameters of permeability and porosity in goafs should be replaced by variable coefficients. The results obtained so far will make it possible to assess to what extent the variability of goaf's properties affects the flow. Additionally, the numerical model will take into account the flow of air and methane mixture, with the methane source located in the goafs. Due to low airflow velocity in the goafs, the numerical calculations should be significantly extended. Assuming the length of the goafs equal to 90.0 m and average airflow velocity in the goafs of 0.001 m/s, the transition of the air and methane mixture from longwall inlet to longwall outlet should be 90 000 s.

Acknowledgements

This paper presents results of the statutory research of the IMG-PAN Institute in year 2020.

References

[1] Ansys Inc, Ansys Fluent Theory Guide. Ansys Inc (2019).

[2] M. Baścik, 3D laser scanning in underground mines – practical experience. School of Underground Mining 2013. The Mineral And Energy Economy Research Institute of Polish Academy of Sciences (2013).

[3] P.Y. Chou, On velocity correlations and the solutions of the equations of turbulent fluctuations. Quarterely of Applied Mathematics (1945).

[4] N.S. Dhamakar, G.A. Blasdell, A.S. Lyrintzis, An Overview of Turbulent Inflow Boundary Conditions for large Eddy Simulations. Proc of the 22 nr AIAA Computational Fluid Dynamics Conference AIAA Paper (2015).

[5] W. Dziurzyński, Prognozowanie procesu przewietrzania kopalni głębinowej w warunkach pożaru podziemnego. Instytut Gospodarki Surowcami Mineralnymi i Energią PAN, Kraków (1998).

[6] J. Janus, PhD thesis, Modelling of flow phenomena in mine drifts using the results of laser scanning. Strata Mechanics Research Institute of Polish Academy of Sciences (2018).

[7] J. Janus, The Application of laser scanning in the process of constructing a mine drift numerical model. 24th World Mining Congress PROCEEDINGS – Underground Mining, Brazilian Mining Association, Rio de Janeiro (2016).

[8] J. Janus, The application of laser scanning in the process of construction a mine drift numerical model. Transactions of the Strata Mechanics Research Institute **18**, 3 (2016).

[9] J. Janus, Assessment of the possibilities of using laser scanning for numerical models constructions. Transactions of the Strata Mechanics Research Institute **17**, (1-2) (2015).

[10] J. Janus, Wpływ zapory przeciwwybuchowej wodnej na pole prędkości i warunki przewietrzania wyrobiska kopalnianego. Archives of Mining Sciences, Seria: Monografia, Nr 19 (2019).

[11] J. Janus, J. Krawczyk, An Analysis of the Mixing of Air and Methane in the Stream Produced by the Mine Injector Station – Present Results of Measurements and Modeling. The Australian Mine Ventilation Conference 2013, The Australian Institute of Mining and Metallurgy (2013).

[12] J. Janus, J. Krawczyk, Measurement and Simulation of Flow in a Section of a Mine Gallery. Energies **14**, 4894 (2021). DOI: https://doi.org/10.24425/ather.2019.128295

[13] J. Janus, J. Krawczyk, The numerical simulation of a sudden inflow of methane into the end segment of a longwall with Y – type ventilation system. Archives of Mining Sciences **59**, (4) (2014).

[14] A. Kidybiński, Podstawy geotechniki kopalnianej. Wydawnictwo Śląsk, Katowice (1982).

[15] J. Krawczyk, J. Janus, An example of defining boundary conditions for a flow in a mine gallery. Abstract in the XXIII Fluid Mechanics Conference Materials, Zawiercie (2018).

[16] J. Krawczyk, J. Janus, Velocity field in the area of artificially generated barrier on the mine drift floor. Przegląd Górniczy **71**, (11) (2015).

[17] J. Krawczyk, Single and multiple-dimensional models of unsteady air and gas flows in underground mines. Archives of Mining Sciences, Seria: Monografia, No 2 (2007).

[18] F. Menter, Turbulence Modeling for Engineering Flows. ANSYS 2012 Inc. (2012).

[19] F. Menter, Best Practice – Scale-Resolving Simulations in ANSYS CFD – Application Brief Version 2.0 (2015).

[20] J. Pokorný, L. Brumarová, P. Kučera, J. Martinka, A. Thomitzek, P. Zapletal, The effect of Air Flow Rate on Smoke Stratification in Longitudinal Tunnel Ventilation. Acta Montanistica Slovaca **24**, (3) (2019).

[21] T. Ren, R. Balusu, C. Claassen, Computational Fluid Dynamics Modelling of Gas Flow Dynamics in Large Longwall Goaf Areas. 35th APCOM Symposium (2011).

[22] P. Skotniczny, Three-Dimensional Numerical Simulation of the Mass Exchange Between Longwall Headings and Goafs, in the Presence of Methane Drainage in A U-Type Ventilated Longwall. Archives of Mining Sciences **58**, (3) (2013).

[23] V. Sokoła-Szewioła, J. Wiatr, Application of laser scanning method for the elaboration of digital spatial representation of the shape of underground mining excavation. Przegląd Górniczy **8** (2013).

[24] J. Szlązak, PhD thesis, Wpływ uszczelniania chodników przyścianowych na przepływ powietrza przez zroby. AGH Kraków (1980).

[25] N. Szlązak, J. Szlązak, Wentylacja wyrobisk ścianowych w kopalniach węgla kamiennego, w warunkach zagrożenia metanowego i pożarowego. Górnictwo i Geologia (2) (2019).

[26] K. Wierzbiński, Wpływ geometrii chodnika wentylacyjnego i sposobu jego likwidacji na rozkład stężenia metanu w rejonie wylotu ze ściany przewietrzanej sposobem U w świetle obliczeń numerycznych CFD. Zeszyt Naukowy Instytutu Gospodarki Surowcami Mineralnymi i Energią Polskiej Akademii Nauk, No 94 (2016).

[27] M.A. Wala, S. Vytla, C.D. Taylor, G. Huang, Mine face ventilation: a comparison of CFD results against benchmark experiments for the CFD code validation. Mining Engineering (2007).

[28] D.M. Worrall, E.W. Wachel, U. Ozbay, D.R. Munoz, J.W. Grubb, Computational fluid dynamic modeling of sealed longwall gob in underground coal mine – A progress report. 14th United States/North American Mine Ventilation Symposium, Calizaya & Nelson (2012).